nature materials

LETTERS

PUBLISHED ONLINE: 12 SEPTEMBER 2010 | DOI: 10.1038/NMAT2835

Nanowire active-matrix circuitry for low-voltage macroscale artificial skin

Kuniharu Takei[1,2,3], Toshitake Takahashi[1,2,3], Johnny C. Ho[1,2,3], Hyunhyub Ko[1,2,3†], Andrew G. Gillies[4], Paul W. Leu[1,2,3], Ronald S. Fearing[1] and Ali Javey[1,2,3*]

Large-scale integration of high-performance electronic components on mechanically flexible substrates may enable new applications in electronics, sensing and energy[1–8]. Over the past several years, tremendous progress in the printing and transfer of single-crystalline, inorganic micro- and nanostructures on plastic substrates has been achieved through various process schemes[5–10]. For instance, contact printing of parallel arrays of semiconductor nanowires (NWs) has been explored as a versatile route to enable fabrication of high-performance, bendable transistors and sensors[11–14]. However, truly macroscale integration of ordered NW circuitry has not yet been demonstrated, with the largest-scale active systems being of the order of 1 cm^2 (refs 11,15). This limitation is in part due to assembly- and processing-related obstacles, although larger-scale integration has been demonstrated for randomly oriented NWs (ref. 16). Driven by this challenge, here we demonstrate macroscale (7 × 7 cm^2) integration of parallel NW arrays as the active-matrix backplane of a flexible pressure-sensor array (18 × 19 pixels). The integrated sensor array effectively functions as an artificial electronic skin[2,17,18], capable of monitoring applied pressure profiles with high spatial resolution. The active-matrix circuitry operates at a low operating voltage of less than 5 V and exhibits superb mechanical robustness and reliability, without performance degradation on bending to small radii of curvature (2.5 mm) for over 2,000 bending cycles. This work presents the largest integration of ordered NW-array active components, and demonstrates a model platform for future integration of nanomaterials for practical applications.

Development of a robust and low-power artificial skin that can detect the environment through touch is of profound interest for robotic and prosthetic applications. Artificial electronic skin (e-skin) requires large-scale integration of pressure-sensitive components with an active-matrix backplane on a thin plastic support substrate. Previously, organic transistors have been used for the active-matrix backplane of e-skin, demonstrating the feasibility of the concept[2,17,18]. Although organic molecules provide promising material systems for flexible electronics, their relatively low carrier mobility often requires large operating voltages (although significant improvements and advancements have been made in recent years). Inorganic crystalline semiconductors, such as NWs, present an advantage as they exhibit high carrier mobilities with superb mechanical flexibility arising from their miniaturized dimensions. To take advantage of their unique physical properties, however, uniform assembly of ordered NW arrays is needed. Here, we used our previously reported contact-printing method[10,11,14] to assemble Ge/Si core/shell NW arrays on a polyimide substrate followed by device fabrication processing. The process scheme for the e-skin device with an integrated NW active-matrix backplane is shown in Fig. 1a and Supplementary Fig. S1, with the process details described in the Methods section.

Optical images of a fully fabricated e-skin, consisting of a 19 × 18 pixel matrix with an active area of 7 × 7 cm^2, are shown in Fig. 1b,c. The structure can easily be bent or rolled to a small radius of curvature, demonstrating the superb mechanical flexibility of the substrate and its integrated electronic components. The sensor array employs an active-matrix circuitry as shown in Fig. 1d. Each pixel is connected to a NW-array field-effect transistor (FET) that actively maintains the pixel state while other pixels are addressed. This presents an important advantage over passive-matrix circuitry where the sensor element itself must maintain its state without the use of an active switching device. Parallel arrays of NWs are used as the channel material of the active-matrix FETs, thereby markedly reducing the stochastic device-to-device variation. The scanning electron micrographs of printed Ge/Si NW arrays are shown in Fig. 1e,f, depicting the well-aligned and uniform NW assembly with a density of ~5 NWs μm^{-1} on the flexible polyimide support substrate. The high degree of alignment and uniformity for the contact-printed NW arrays is critical to achieve high-performance and large-scale electronics that are configured as functional systems at such a high degree of complexity. A laminated pressure-sensitive rubber (PSR) is used as the sensing element[17,18]. The source electrodes of NW-array FETs are connected to ground through the PSR. By applying an external pressure, the conductance of PSR changes, resulting in the modulation of NW FET characteristics and thus the pixel output signal. The gate (V_{GS}) and drain (V_{DS}) bias of FETs are used for addressing the word (that is, row) and bit (that is, column) lines of the matrix, respectively. By addressing and monitoring the conductance of each pixel in the active matrix, spatial mapping of the applied pressure can readily be attained.

The electrical properties of Ge/Si NW-array FETs on a polyimide substrate, before the lamination of PSR, are shown in Fig. 2. The devices exhibit p-type behaviour with a high ON-current, $I_{ON} \sim 1$ mA at $V_{DS} = 3$ V (Fig. 2a,b). The peak field-effect mobility for the device is ~20 cm^2 V^{-1} s^{-1}, as estimated from the measured transconductance ($g_m \sim 55$ μS) at $V_{DS} = 0.5$ V and electrostatically modelled capacitance ($C_{ox} \sim 0.49$ pF; assuming a NW density of 5 NW μm^{-1}). The performance of NW-array FETs reported here is about 10 times higher than their organic counterparts, although

[1]Department of Electrical Engineering and Computer Sciences, University of California at Berkeley, Berkeley, California 94702, USA, [2]Berkeley Sensor and Actuator Center, University of California at Berkeley, Berkeley, California 94720, USA, [3]Materials Sciences Division, Lawrence Berkeley National Laboratory, Berkeley, California 94720, USA, [4]Department of Mechanical Engineering, University of California at Berkeley, Berkeley, California 94702, USA. †Present address: School of Nano-Biotechnology & Chemical Engineering, Ulsan National Institute of Science and Technology, Ulsan Metropolitan City 689-798, South Korea. *e-mail: ajavey@berkeley.edu.

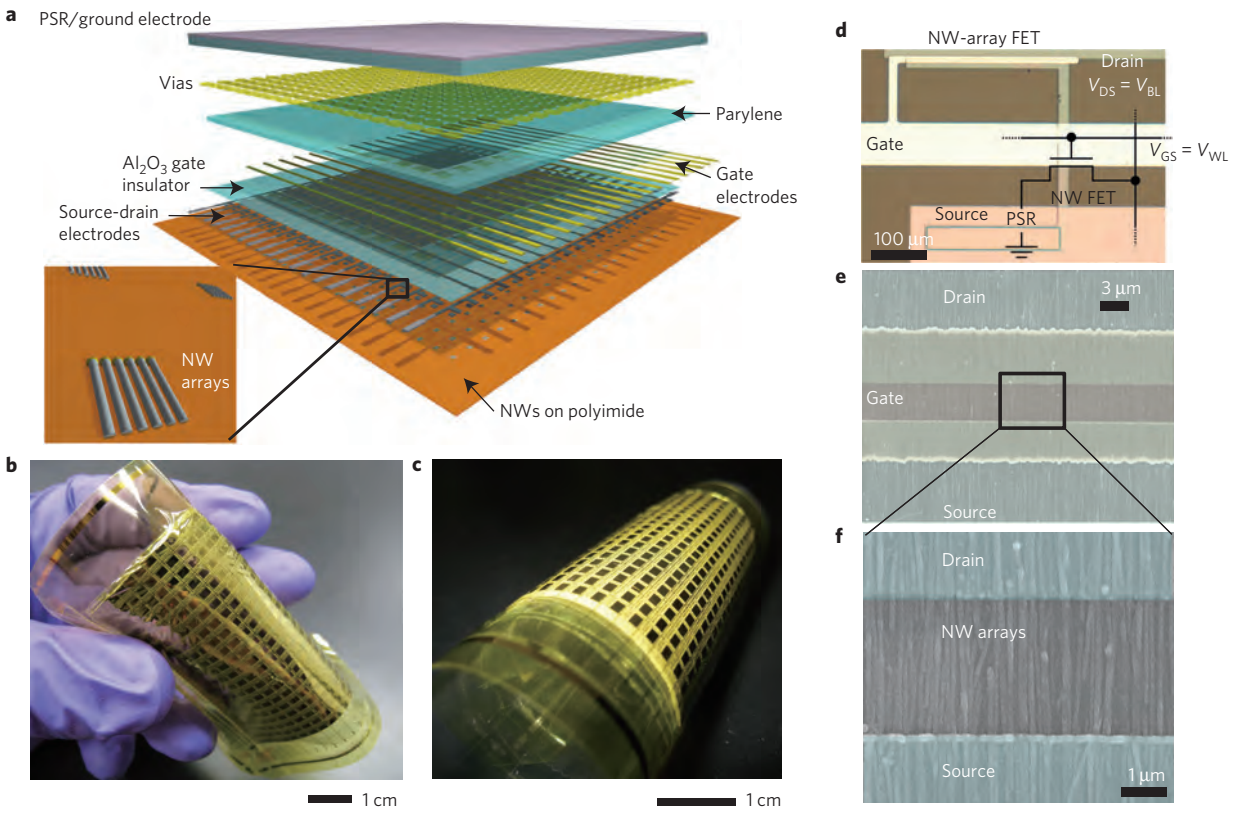

Figure 1 | Nanowire-based macroscale flexible devices. a, Schematic of the passive and active layers of NW e-skin (see Methods). **b**,**c**, Optical photographs of a fully fabricated e-skin device (7×7 cm^2 with a 19×18 pixel array) under bending (**b**) and rolling (**c**) conditions. **d**, Optical-microscope image of a single sensor pixel in the array, depicting a Ge/Si NW-array FET (channel length ~3 μm, channel width ~250 μm) integrated with a PSR. The circuit structure for the pixel is also shown. **e**,**f**, Scanning electron micrographs of a NW-array FET, showing the high degree of NW alignment and uniformity achieved by contact printing with a density of ~5 NWs μm^{-1}.

future improvements may still be achieved by using more optimal NW materials[19,20]. For instance, we have previously shown that printed InAs NW arrays exhibit a peak field-effect mobility of ~600 cm^2 V^{-1} s^{-1} (ref. 14). Nevertheless, the performance of the Ge/Si NWs used in this work is adequate for the low-power, active-matrix backplane of the proposed sensor application. When integrated with PSR, NW-array FETs exhibit high sensitivity to an applied normal pressure for $P = 0$–15 kPa (Fig. 2c). This sensitivity arises from the conductance change of the PSR on an applied pressure owing to the shortened tunnelling path between the conductive carbon nanoparticles embedded in the rubber. Specifically, the ON-state conductance of NW-array FETs, G_{NW-ON}, shows an exponential pressure dependency for $P < \sim 2$ kPa, beyond which the dependence is linear up to the maximum applied pressure of ~15 kPa (Fig. 2d). The reduced sensitivity at high pressures arises from the reduced elastic modulus of the rubber. In the linear operation regime, the sensor sensitivity, $S = dG_{NW-ON}/dP$, is ~11.5 μS kPa^{-1}. For our device concept, the PSR effectively serves as a tunable resistor in series with the NW-array FET. An important design consideration is to ensure that the ON-conductance of the NW arrays is higher than that of the PSR (G_{PSR}) under all operating conditions. In our case, $G_{NW-ON} \sim 0.35$ mS and $G_{PSR} = 1$ μS–0.15 mS (per pixel, 1.9×1.2 mm^2 cross-sectional area) for an applied pressure of 0–15 kPa.

To shed light on the response and relaxation time constants of the e-skin device, time-resolved measurements were carried out (Fig. 3). A computer-controlled stepping motor and a force sensor were used to apply an external pressure of ~15 kPa with a frequency of up to 5 Hz while measuring the electrical response of a pixel (Fig. 3a). A response and relaxation time of $< \sim 0.1$ s was observed. The measured time constants are approximately the same as that of the input pressure profile (Fig. 3b), suggesting that they are limited at present by the experimental set-up rather than the mechanical response of the PSR. Furthermore, the response was measured as a function of the frequency of the applied pressure. Figure 3c illustrates the output electrical signal of a pixel and the applied pressure profile with a frequency of 1, 3 and 5 Hz. Clearly, the devices are responsive without a significant signal degradation up to 5 Hz, which demonstrates the fast and deterministic response of the e-skin device.

Next, to examine the mechanical flexibility and robustness of the sensor array—which are important figures of merit for e-skin applications—we examined a single-pixel output conductance when the array was bent, and after repetitive cycles of bending stress. Figure 4a shows the normalized change in the conductance, $\Delta G/G_o$, where $\Delta G = G_o - G$; G and G_o are the conductance for the bent and relaxed (that is curvature radius is infinity) states, respectively, of a single representative pixel as a function of the bending radius, down to 2.5 mm. The sample was bent along the axial direction of the aligned NWs as schematically illustrated in the inset of Fig. 4a. Clearly, the output conductance exhibits minimal change on bending with $\Delta G/G_o \sim 6\%$ for a radius of curvature of 2.5 mm. Next, the mechanical reliability and robustness of the flexible sensor array were tested by measuring the conductance as a function of bending cycles, up to 2,000 times. For this experiment, the sensor substrate was bent to a radius <10 mm and relaxed multiple times followed by electrical characterization. The normalized conductance change, $\Delta G/G_o$, as a function of the number of bending cycles is shown in Fig. 4b, exhibiting minimal performance degradation even after 2,000 cycles and demonstrating

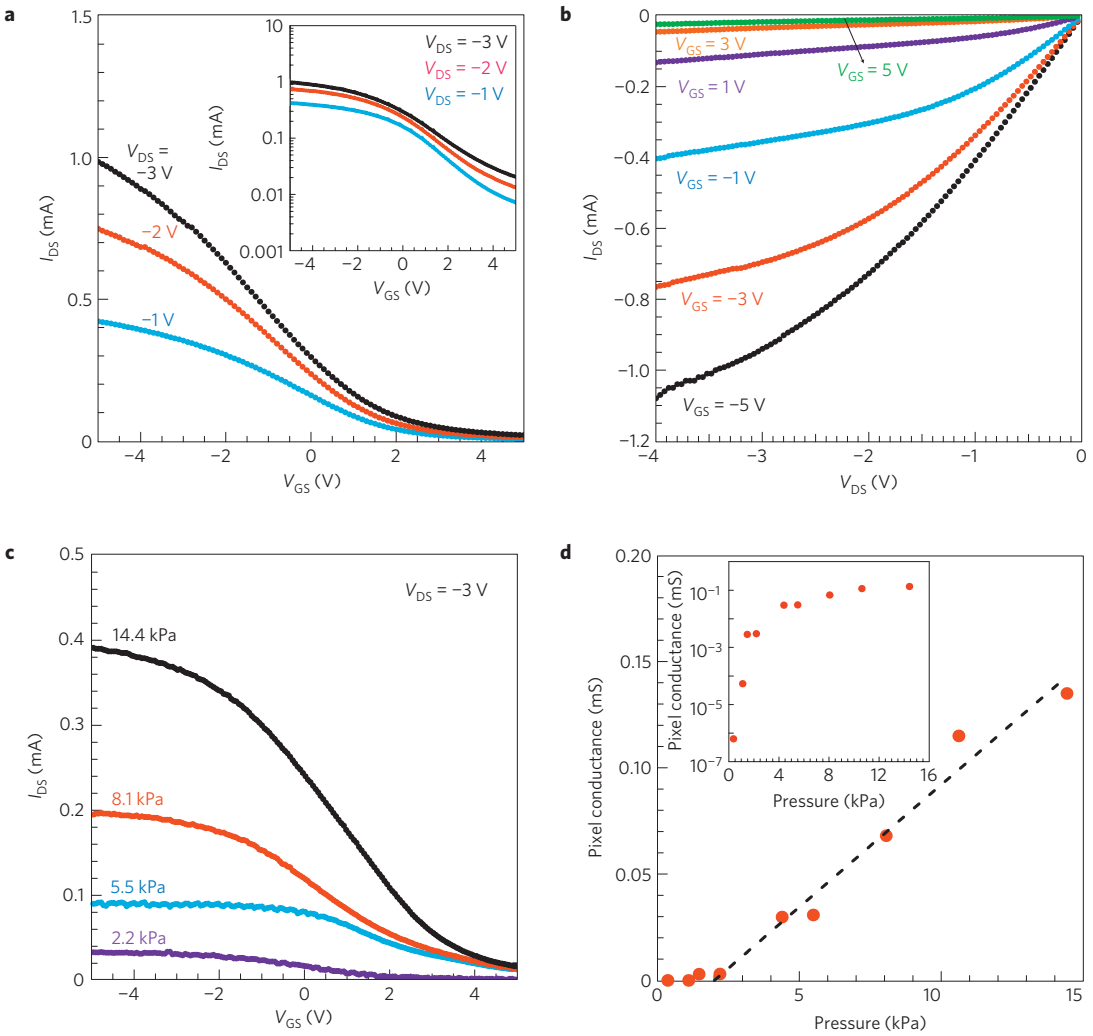

Figure 2 | Electrical characterization of NW-array FETs. a,**b**, Output and transfer characteristics of a representative NW FET on a polyimide substrate, before the lamination of the PSR. **c**, I_{DS}–V_{GS} curves as a function of an applied pressure for a representative pixel after the lamination of the PSR. In this case, the source electrode of the NW-array FET is connected to ground through the rubber. **d**, The pressure dependence of the pixel output conductance at $V_{GS} = V_{DS} = -3$ V. The log-scale plot is show in the inset.

the mechanical robustness of the devices. This excellent reliability is because of the miniaturized dimensions of NWs (30 nm diameter) and metal thin films (50–100 nm thick), which make the arrays highly flexible, without susceptibility to cracking and/or peeling from the flexible support substrate. These results demonstrate that the mechanical robustness of the NW-based devices is sufficient for highly versatile and mechanically flexible e-skin applications.

To shed further light on the mechanical robustness of the flexible NW-array devices, the induced strain on bending was calculated by using a finite-element method simulation (Comsol Multiphysics 3.3) as shown in Fig. 4c. The substrate is mechanically bent to a 2.5 mm radius of curvature. The device is assumed to be in a state of plane strain with a symmetric right boundary condition. From the simulation, the top and bottom surfaces of the substrate have maximum strains $\varepsilon_{xx} \sim 1$ and -1%, respectively. Although the device is near the top of the substrate, far from the neutral axis of bending, the strain in the active regions is relatively low. The Young's moduli of the NW, dielectric material and metal are about two orders of magnitude greater than those of the polyimide and parylene support layers, resulting in a non-uniform strain distribution near the device. Furthermore, as the dimensions of the NWs and metal lines are small (sub 100-nm thickness), most of the strain in the overall substrate is accommodated by the parylene and polyimide layers. As seen in Fig. 4c, there is a maximum strain of ~1% in the parylene layer near the corner of the metal gate. The NW encounters a strain of only ~0.35% along its length. In practice, the NWs have even less strain than this value because of the assumption of plane strain used in the simulations. The simulation results explain the mechanical robustness of the sample under large bending, as the transistors undergo minimal strain. This also explains the lack of bending dependency of the pixel electrical characteristics even for small radii of curvature (down to ~2.5 mm). In the future, placing the devices closer to the neutral axis of the substrate would subject the devices to smaller strain under bending.

Finally, the scalability of the proposed process scheme is demonstrated by the successful fabrication of a 19 × 18 pixel array e-skin, with a physical size of 7 × 7 cm^2. This presents the largest-scale integration of ordered NW components for electronic and sensing applications, with a 5–10 times increase in the area of the active device region over previous works[11,15]. To demonstrate the functionality of the integrated e-skin, a piece of polydimethylsiloxane (PDMS) moulded as the letter '*C*' with an area of ~3 cm^2 is placed on top of the sensor array, followed by the application of a normal pressure of ~15 kPa (Fig. 5a). The elastic PDMS mould enables the uniform distribution of the pressure over an area corresponding to that of the '*C*'. The word

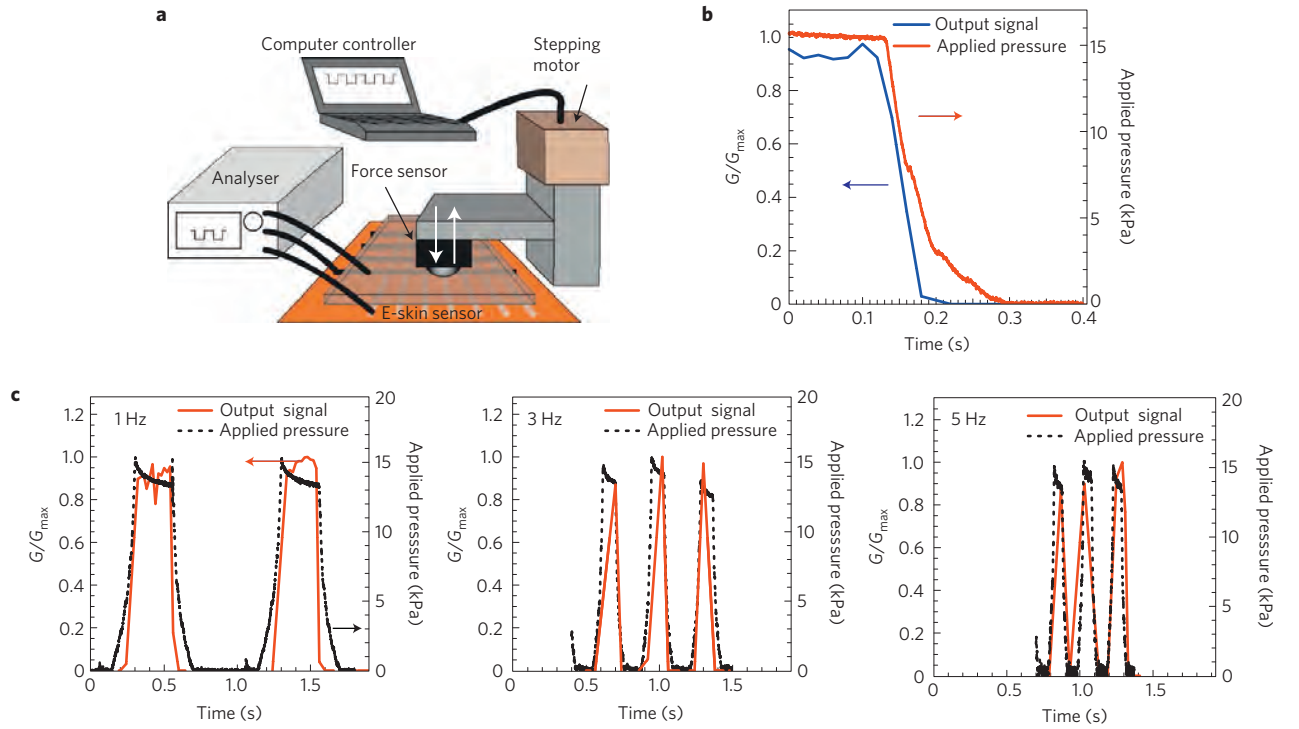

Figure 3 | Time-resolved measurements of the sensor response. a, Schematic of the experimental set-up. A stepping motor and a force sensor controlled by a computer were used to control the applied pressure and frequency while the output signal was recorded at $V_{DS} = 3$ V and $V_{GS} = -5$ V. **b**, Normalized output signal of a pixel during the relaxation step (that is, when the pressure is released), showing a response time of <0.1 s. The output signal is normalized by the maximum conductance, G_{max}, of the pixel at 15 kPa. The applied pressure profile is also shown. **c**, Time-resolved measurements of the output signal for an applied pressure frequency of 1 Hz (left), 3 Hz (middle) and 5 Hz (right).

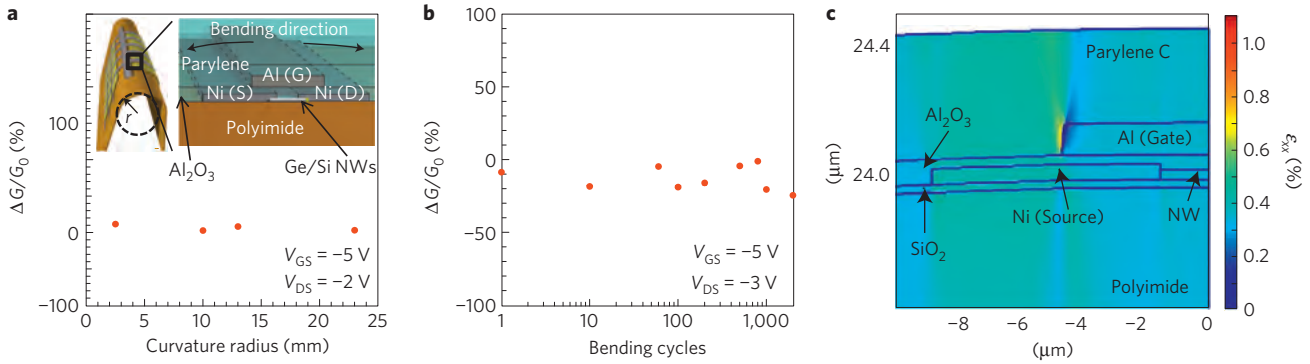

Figure 4 | Mechanical testing of integrated pressure-sensor devices. a, The normalized conductance change, $\Delta G/G_o$, of a representative pixel at different curvature radii. The insets illustrate the device structure and bending orientation used in the experiments. **b**, $\Delta G/G_o$ as a function of mechanical bending cycles, demonstrating the mechanical robustness of the devices with minimal performance degradation even after 2,000 cycles of bending and relaxing. **c**, Theoretical simulation of the strain for a NW device when bent to a 2.5 mm curvature radius. A symmetric right boundary condition is assumed in the simulation; therefore, only half of the device is shown.

and bit line voltages of $V_{WL} = 5$ V and $V_{BL} = 0.5$ V are applied, respectively, to address each pixel individually (Fig. 5b). The output conductance for each individual pixel is measured, and plotted as a two-dimensional intensity plot (Fig. 5d). The yield of functional active pixels was 84% with the defective pixels being mainly caused by the failure of the process integration steps (for example, shortage and/or breakage of metal lines owing to poor lithography and/or lift-off) and imperfect NW printing (for example, insufficient NW transfer at local sites induced by a dust particle). As depicted in Fig. 5d, the applied pressure profile can be spatially resolved by the integrated NW e-skin. The pixel resolution used in this work was set to ~2.5 mm to enable a manageable number of pixels without the need to implement system integration for the signal readout. Although the pixel size used here clearly demonstrates the feasibility of the presented approach for e-skin applications, in the future, the pixel size can be readily reduced down to the lithographic limits (for example, sub-2 μm for photolithography) to enable imaging with higher spatial resolution. Notably, the e-skin functionality is achieved with low operating voltages ($V_{BL} =$ 0.5–3 V and $V_{WL} = 2$–5 V). Further scaling of the operating voltage can be achieved by reducing the device dimensions, such as the gate dielectric thickness, which limits the operating voltage of the circuit at present.

The ability to controllably achieve functional electronics on truly macroscales using printed NW arrays presents a feasible route towards their implementation for practical applications.

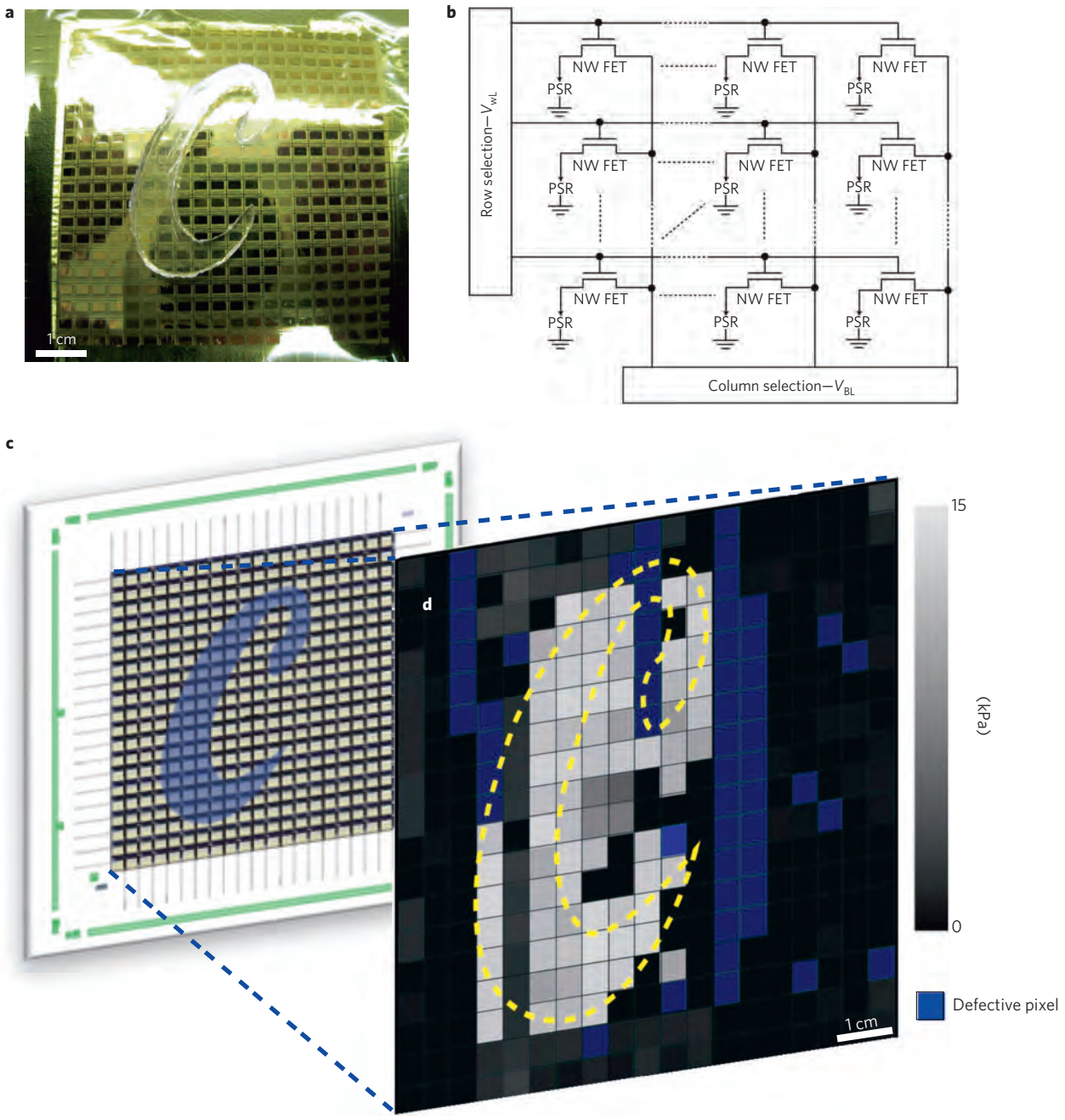

Figure 5 | Fully integrated, artificial e-skin with NW active-matrix backplane. a, Photograph of a fabricated e-skin with a PDMS mould in the shape of '*C*' placed on the top for applying pressure and subsequent imaging. **b**, Circuit schematic of the active matrix to address individual pixels by applying row (V_{BL}) and column (V_{WL}) signals. **c**, Design layout of the sensor device. **d**, The corresponding two-dimensional intensity profile obtained from experimental mapping of the pixel signals. The character '*C*', corresponding to the applied pressure profile, can be readily imaged by the e-skin.

The artificial e-skin demonstrated here presents just one example of the type of system that can be fabricated by using the reported process scheme. Notably, the single-crystalline nature of the inorganic NWs enables low-voltage operation with high device stability, which presents an important advantage in their use for electronic and sensory applications over conventional thin-film transistor technologies. Furthermore, their small dimensions (for example, diameter ~30 nm) make them highly flexible with superb mechanical reliability and robustness. From the cost perspective, the ability to synthesize and print single-crystalline structures, without the use of crystalline wafers and/or complex epitaxial growth processes is highly attractive. Although batch-to-batch processing was used in this work, in the future, roll-to-roll processing may be possible for the large-scale fabrication of low-cost NW sensor circuitry.

Methods

Device fabrication. An approximately 24-μm-thick polyimide layer (PI-2525, HD MicroSystems) is spin-coated on a handling silicon wafer, followed by electron-beam evaporation of ~25 nm SiO_x. Subsequently, vapour–liquid–solid grown Ge/Si core/shell NW parallel arrays are transferred to the lithographically predefined active regions by a contact-printing method (see Supplementary Information for process details), as described in detail in our previous reports[10,11,14]. Afterwards, source and drain electrodes with a channel length $L \sim 3$ μm and width $W \sim 250$ μm are defined by photolithography and deposition of a Ni thin film (~50 nm). Next, a ~50-nm-thick Al_2O_3 layer is deposited by atomic layer deposition as the gate dielectric followed by the fabrication of the Al top-gate electrodes (~100 nm) by thermal evaporation and lift-off. An insulating layer of

parylene-C (~500 nm) is then deposited on the active matrix, and via-holes are patterned by oxygen plasma etching to contact the source electrode of each NW FET. The vias are then connected to photolithographically patterned Ni pads (1,900 × 1,200 μm, ~50 nm thick) on the top surface of parylene. These Ni pads provide electrical interfaces between the underlying transistors and a silicone-based PSR (PCR Technical), which is laminated on top of the substrate. An aluminium layer on the top surface of the PSR serves as the ground electrode. Finally, the polyimide substrate with the fabricated circuitry is peeled off from the handling wafer, resulting in a highly flexible and fully integrated e-skin.

Received 26 March 2010; accepted 16 July 2010; published online 12 September 2010

References

1. Cao, Q. *et al.* Medium-scale carbon nanotube thin-film integrated circuits on flexible plastic substrates. *Nature* **454,** 495–500 (2008).
2. Sekitani, T. *et al.* Organic nonvolatile memory transistors for flexible sensor arrays. *Science* **326,** 1516–1519 (2009).
3. Cohen-Karni, T., Timko, B. P., Weiss, L. E. & Lieber, C. M. Flexible electrical recording from cells using nanowire transistor arrays. *Proc. Natl Acad. Sci. USA* **106,** 7309–7313 (2009).
4. Fan, Z. *et al.* Three-dimensional nanopillar-array photovoltaics on low-cost and flexible substrates. *Nature Mater.* **8,** 648–653 (2009).
5. McAlpine, M. C., Ahmad, H., Wang, D. & Heath, J. R. Highly ordered nanowire arrays on plastic substrates for ultrasensitive flexible chemical sensors. *Nature Mater.* **6,** 379–384 (2007).
6. Park, S-I. *et al.* Printed assemblies of inorganic light-emitting diodes for deformable and semitransparent displays. *Science* **325,** 977–981 (2009).
7. Rogers, J. A. & Huang, Y. A curvy, stretchy future for electronics. *Proc. Natl Acad. Sci. USA* **106,** 10875–10876 (2009).
8. Yoon, J. *et al.* Ultrathin silicon solar microcells for semitransparent, mechanically flexible and microconcentrator module designs. *Nature Mater.* **7,** 907–915 (2008).
9. Javey, A., Nam, S., Friedman, R. S., Yan, H. & Lieber, C. M. Layer-by-layer assembly of nanowires for three-dimensional, multifunctional electronics. *Nano Lett.* **7,** 773–777 (2007).
10. Fan, Z. *et al.* Wafer-scale assembly of highly ordered semiconductor nanowire arrays by contact printing. *Nano Lett.* **8,** 20–25 (2008).
11. Fan, Z., Ho, J. C., Jacobson, Z. A., Razavi, H. & Javey, A. Large scale, heterogeneous integration of nanowire arrays for image sensor circuitry. *Proc. Natl Acad. Sci. USA* **105,** 11066–11070 (2008).
12. Takahashi, T. *et al.* Monolayer resist for patterned contact printing of aligned nanowire arrays. *J. Am. Chem. Soc.* **131,** 2102–2103 (2009).
13. Yerushalmi, R., Jacobson, Z. A., Ho, J. C., Fan, Z. & Javey, A. Large scale, highly ordered assembly of nanowire parallel arrays by differential roll printing. *Appl. Phys. Lett.* **91,** 203104 (2007).
14. Fan, Z. *et al.* Towards the development of printable nanowire electronics and sensors. *Adv. Mater.* **21,** 3730–3743 (2009).
15. Qing, Q. *et al.* Nanowire transistor arrays for mapping neural circuits in acute brain slices. *Proc. Natl Acad. Sci. USA* **107,** 1882–1887 (2010).
16. Ju, S. *et al.* Transparent active matrix organic light-emitting diode displays driven by nanowire transistor circuitry. *Nano Lett.* **8,** 997–1004 (2008).
17. Someya, T. *et al.* A large-area, flexible pressure sensor matrix with organic field-effect transistors for artificial skin applications. *Proc. Natl Acad. Sci. USA* **101,** 9966–9970 (2004).
18. Someya, T. *et al.* Conformable, flexible, large-area networks of pressure and thermal sensors with organic transistor active matrixes. *Proc. Natl Acad. Sci. USA* **102,** 12321–12325 (2005).
19. Xiang, J. *et al.* Ge/Si nanowire heterostructures as high-performance field-effect transistors. *Nature* **441,** 489–493 (2006).
20. Ford, A. C. *et al.* Diameter-dependent electron mobility of InAs nanowires. *Nano Lett.* **9,** 360–365 (2009).

Acknowledgements

This work was partially financially supported by NSF CAREER Award, MARCO/MSD Focus Center and DARPA/DSO Programmable Matter. The synthesis part of this work was supported by a LDRD from Lawrence Berkeley National Laboratory. A.J. acknowledges support from the World Class University programme at Sunchon National University.

Author contributions

K.T., T.T. and A.J. designed the experiments. K.T., T.T., A.G.G., J.C.H. and H.K. carried out experiments. K.T. and P.W.L. carried out simulations. K.T., T.T., P.W.L. and A.J. contributed to analysing the data. K.T. and A.J. wrote the Letter and all authors provided feedback.

Additional information

The authors declare no competing financial interests. Supplementary information accompanies this paper on www.nature.com/naturematerials. Reprints and permissions information is available online at http://npg.nature.com/reprintsandpermissions. Correspondence and requests for materials should be addressed to A.J.

nature materials

SUPPLEMENTARY INFORMATION

DOI: 10.1038/NMAT2835

Supplementary Information

Nanowire active matrix circuitry for low-voltage macro-scale artificial skin

Kuniharu Takei[1,2,3], Toshitake Takahashi[1,2,3], Johnny C. Ho[1,2,3], Hyunhyub Ko[1,2,3], Andrew G. Gillies[4], Paul W. Leu[1,2,3], Ronald S. Fearing[1], Ali Javey[1,2,3]*

[1]Department of Electrical Engineering and Computer Sciences, University of California at Berkeley, Berkeley, California 94702, USA.

[2]Berkeley Sensor and Actuator Center, University of California at Berkeley, Berkeley, California 94720, USA.

[3]Materials Sciences Division, Lawrence Berkeley National Laboratory, Berkeley, California 94720, USA.

[4]Department of Mechanical Engineering, University of California at Berkeley, Berkeley, California 94702, USA.

* Correspondence should be addressed to A.J. (ajavey@berkeley.edu).

DOI: 10.1038/NMAT2835

Materials and Methods

Nanowire growth

Ge/Si core/shell NWs were grown by Au-catalyzed vapor-liquid-solid method, on a Si/SiO_2 (50 nm, thermally grown) substrate. 10 nm Au colloids immobilized on poly-L-lysine on the substrate serve as a catalyst for Ge NW growth. Ge NWs were grown at 270 ^{o}C with a chamber pressure of 45 torr under a constant flow of 12 sccm GeH_4 gas (10 % diluted in H_2) for 30 min. The grown NWs are ~30 μm long. Without exposing to ambient air, Si shells were grown at 450 ^{o}C and 5 torr under a 5 sccm SiH_4 gas (100 %) flow for 5 mins, resulting in ~5nm thick shell layer on Ge NWs. The Si shells were poly-crystalline.

Nanowire contact printing

PI substrate coated with a photolithographically patterned resist was exposed to a mild O_2 plasma, followed by poly-L-lysine treatment (i.e., drop-casting and rinsing with de-ionized water). After the surface treatment, the PI substrate was mounted on a stage, and a growth substrate with Ge/Si NWs was placed on top in the presence of octane as lubricant. A normal pressure of ~10 g/cm^2 was applied while the growth substrate was directionally slid at a constant velocity of ~20 mm/min on top of the PI substrate. After ~1 mm sliding, an additional normal pressure of ~55 g/cm^2 was applied. The two step process for applying the appropriate pressure results in minimal "stamping of NWs". After contact printing of the NWs, the donor substrate was gently removed from the receiver substrate and the receiver substrate was dried by N_2. Finally, the PI substrate was dipped into acetone to lift-off the resist, resulting in the patterned assembly of NWs. Using this process, the observed density of Ge/Si NWs on polyimide substrate was ~5 NWs/μm as examined by SEM.

Device fabrication

Polyimide (PI-2525) liquid base solution was spin-coated twice on a 4 inch SiO_2/Si handling wafer to achieve a 24 μm thick, flexible support substrate. PI was then cured on a hot plate by first increasing the temperature to 300 ^oC at a rate of ~5 ^oC/min, and then baking at 300 ^oC for 1 hr. Next, ~25 nm-thick SiO_x was deposited by using electron-beam evaporation. Photolithography step was carried out for predefined NW patterning, followed by NW contact printing (Fig. S1A). Subsequently, source and drain electrodes were defined by photolithography and Ni thin film (~50 nm) deposition by thermal evaporation (Fig. S1B). As a gate dielectric, ~50 nm-thick Al_2O_3 (dielectric constant ~8.6) film was deposited by atomic layer deposition (ALD) at 200 ^oC using 500 cycles of 0.1 sec trimethyl-aluminum pulse, 20 sec N_2 purge, 0.2 sec water pulse, and 20 sec N_2 purge. Afterwards, Al top gate electrode (~100 nm, evaporated) was patterned by photolithography and lift-off (Fig. S1C), followed by parylene-C (~500nm) deposition. Parylene-C is used as an insulator layer between the pressure sensitive rubber (PSR; PCR Technical, JAPAN) and active matrix backplane. Via-holes through parylene-C were patterned by oxygen plasma etching to contact the source electrode of each NW FET in the matrix. Photolithographically patterned electrodes (Ni ~50 nm) for each pixel were then deposited to provide an electrical interfacing between underlying transistors and PSR (Fig. S1D). Al foil on the top surface of PCR was laminated on the device (Fig. S1E), and the fully fabricated device was finally peeled off from the Si/SiO_2 handling wafer (Fig. S1F).

DOI: 10.1038/NMAT2835

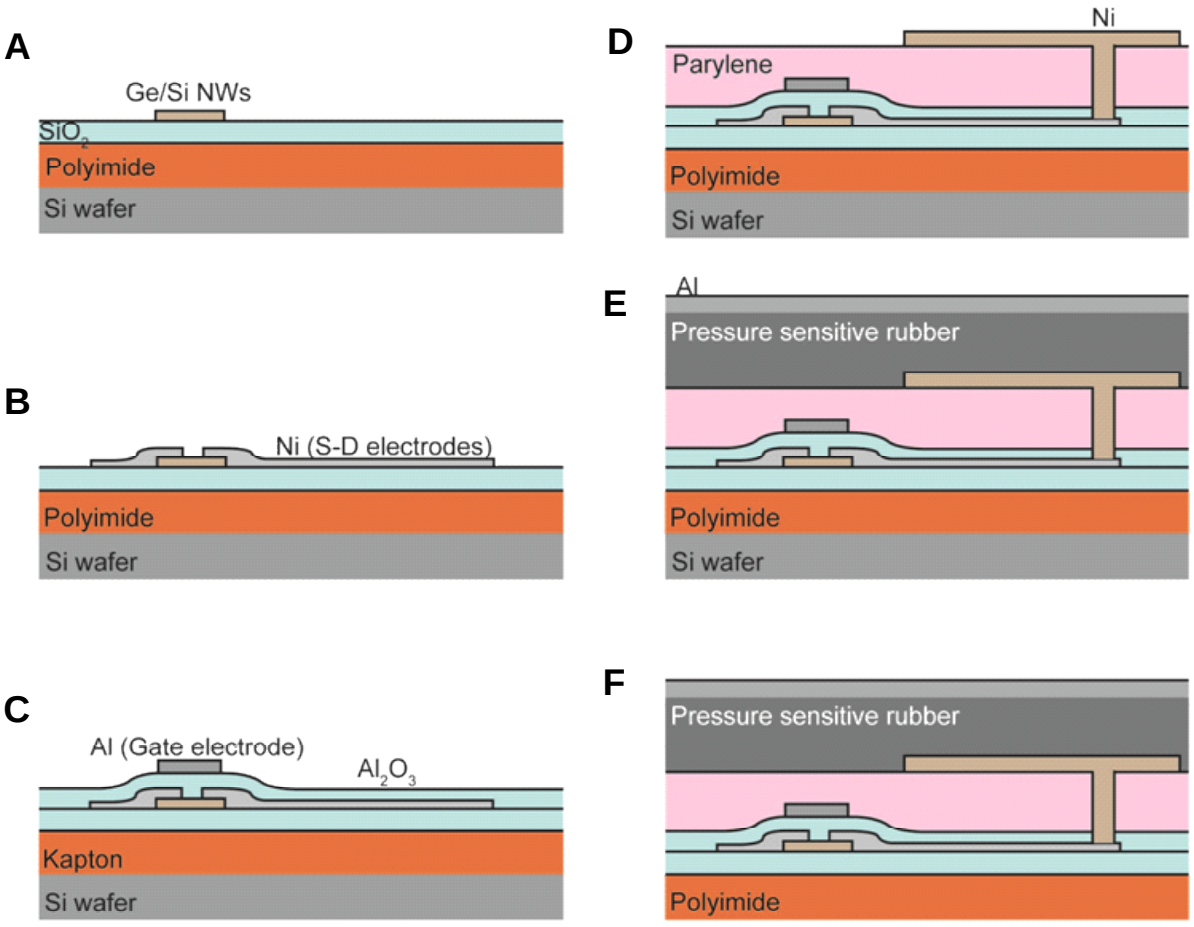

Figure S1. Schematic illustration of the fabrication process for flexible macro-scale e-skin utilizing a NW active matrix backplane.